Current Distributions in Large-Radius Pinch Discharges

ROBERT G. JAHN* AND WOLDEMAR VON JASKOWSKY†
Princeton University, Princeton, N. J.

In an effort to understand more fully the basic mechanisms of gas acceleration in pulsed plasma devices, a series of detailed magnetic probe experiments has been performed on a variety of large-radius linear pinch discharges. From the space and time variations of the interior magnetic fields thus determined, the concomitant distributions of current density within the discharges have been evaluated. For example, in argon at initial pressures between 20 μ and 3 mm, a 10-kv, 230-kc pulse from a 15-μf capacitor bank is found to generate well-defined cylindrical pulses of current which propagate radially inward from the periphery of the electrodes. The observed radius-time trajectories of these pulses, and those of the accompanying luminous fronts, have been compared with theoretical snow-plow calculations and are found to be reconcilable if some fractional "sweeping efficiency" is assigned to each of the observed current pulses. The applicability of the scaling laws implicit in the snow-plow formulation has been explored experimentally by changing the initial pressure, the type of gas, and the radius of the discharge.

Introduction

THE research described in this paper is part of a detailed experimental and theoretical study of various physical processes occurring in a large-radius pinch discharge. Of particular interest are those details of the breakdown initiation, current sheet stability, and magnetogasdynamic acceleration which seem generally relevant to various pulsed plasma propulsion devices. The apparatus employed in the experiments has been developed to generate reproducible, stable, geometrically simple discharges in a form accessible to detailed study. This apparatus and some earlier experimental results have been described in detail in a previous article.[1] Briefly, the central device is an aluminum discharge chamber with plane circular electrodes of 4- or 8-in. diam, separated by a 2-in. gap of test gas at some prescribed pressure (Figs. 1 and 2). The discharge is driven by a circular bank

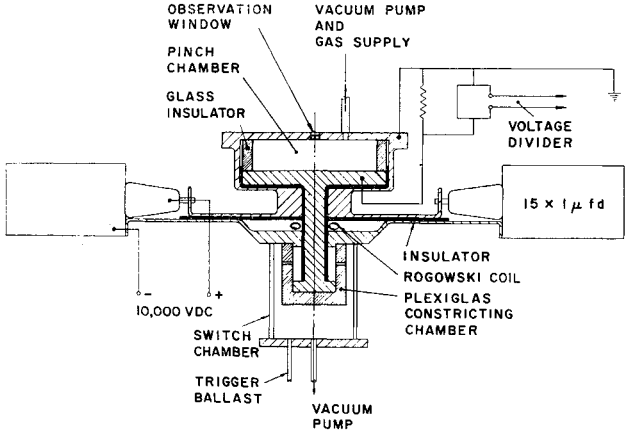

Fig. 1 Plasma pinch apparatus (schematic).

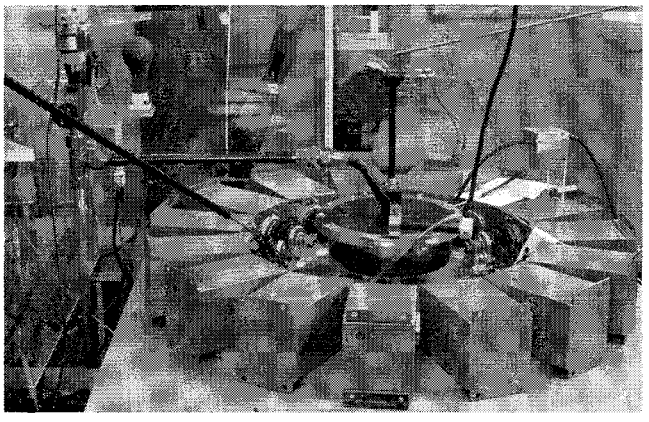

Fig. 2 View of plasma pinch apparatus.

of 15 1.0-μf capacitors charged to 10,000 v, ringing down through a low-inductance circuit via a gas-triggered inverse pinch switch, also described in detail elsewhere.[2] Terminal measurements with a voltage divider and Rogowski coil indicate that the discharge current rises at about 5×10^{11} amp/sec to a peak value of 200,000 amp from which it rings down at about 230 kc, developing some 10% of the bank voltage across the electrode gap.

The luminous phenomena occurring during the discharge are observed by rotating mirror streak photographs taken along a diameter of the chamber, and by single-frame Kerr cell photographs taken through special glass electrodes[1] at selected times. Figure 3 shows a typical streak photograph of an 8-in.-diam discharge in 20 μ argon. The breakdown is seen to initiate at the outer edge of the electrodes, presum-

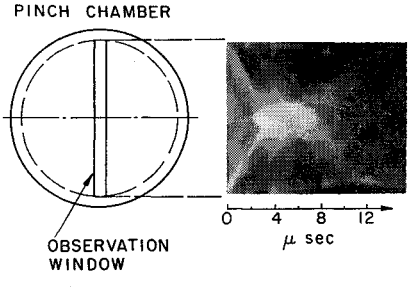

Fig. 3 Streak photograph of 8-in. pinch discharge in 20 μ argon.

Presented as Preprint 64-25 at the AIAA Aerospace Sciences Meeting, New York, January 20–22, 1964; revision received July 2, 1964. This program is supported by NASA Grant NsG-306-63. The authors gratefully acknowledge the work of N. A. Black, R. Burton, J. Corr, and A. L. Casini in performing and interpreting many of the experiments. N. A. Black prepared the Appendix.

* Associate Professor of Aeronautical Engineering, Guggenheim Laboratories for the Aerospace Propulsion Sciences. Member AIAA.

† Research Engineer, Guggenheim Laboratories for the Aerospace Propulsion Sciences.

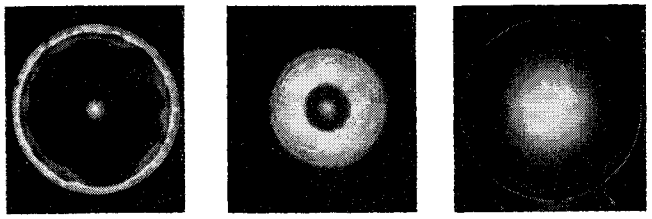

a) 2.3 μsec b) 6.7 μsec c) 11.0 μsec

Fig. 4 Axial photographs of 8-in. pinch discharge in 120 μ argon (0.05-μsec exposure).

ably as a peripheral ring, and then to propagate inward. Subsequent discharges occurring near the times of current reversal in the ringdown pattern are also established at the outer edge of the electrodes, and follow the first luminous front in toward the center.

Full-field Kerr cell photographs, such as those shown in Fig. 4, verify that the luminous fronts are cylindrical in structure with little azimuthal aberration or tendency toward instability. The velocities of these luminous fronts are strong functions of the ambient gas pressure and molecular weight and of the circuit parameters and chamber size. The correlation of their trajectories with the experimentally determined current density and magnetic field distributions and with a theoretical model is the main topic of this paper.

Current Density Distributions

The phenomenological observations of the progress of the luminous fronts permit little interpretation until the development of the current density distributions and their associated magnetic fields within the chamber are established. For this purpose, magnetic probes of the conventional design[3] were introduced at various radial positions within the discharge, midway between the electrodes. These probes are constructed of five turns of 0.25-mm formvar wire, each about 5 mm^2 in cross section, enclosed in a 5-mm-o.d. pyrex tube. The probe tubes are inserted radially through the side wall insulator to the desired position within the chamber. Figure 5 shows the response $(\partial B/\partial t)(t)$ and the integrated response $B(t)$ of one such probe located at radii of 3.0 and 1.5 in. in an 8-in.-diam discharge of 20 μ argon. The series of sharp peaks on the $\partial B/\partial t$ records immediately indicates that the current density, like the luminosity, is localized in relatively thin sheets that propagate radially inward.

Detailed reduction of many magnetic probe records like that shown previously yields maps of the current density distribution as a function of radius at various times in accordance with the appropriate statement of Maxwell's relation in cylindrical geometry:

$$\mu_0 j = (1/r)(\partial/\partial r)(Br)$$

A typical map of this sort, in this case for an 8-in.-diam discharge in 120 μ argon, is shown in Figs. 6a and 6b. The current density is seen to assemble itself into a fairly broad pulse near the outer edge, which then propagates inward at nearly constant amplitude for about $1\frac{1}{2}$ in. At that time, about 2.2 μsec after breakdown, the current in the external circuit reverses, and a new pulse of reverse polarity arises at the outer wall. This second pulse, which also proceeds inward, is seen to be of greater amplitude than the first, even though the external circuit current is now less than during the first half cycle. The second pulse also propagates somewhat faster than the first and eventually reaches about half radius before being "short-circuited" by another rereversal of external current. At this time, a corresponding third positive discharge pulse forms back at the outer wall (not shown in Fig. 6b).

It is speculated that the second pulse owes its sharper definition and greater amplitude to the fact that it propagates into a body of gas already substantially ionized by the passage of the first current sheet, which itself enjoys no such advantage. The higher velocity of the second sheet may arise from a correspondingly higher $\mathbf{j} \times \mathbf{B}$ force acting on it, or from the fact that the first sheet has swept up some of the gas, leaving a lower density medium, which may also be convecting inward, ahead of the second sheet.

Included in Fig. 6 are the trajectories of the luminous fronts for this type of discharge (solid lines), obtained from the streak photographs. The first luminous front is seen to propagate coincidently with the peak of the current density up until the time of current reversal (2.2 μsec), and then to drop somewhat behind. The second luminous front propagates a bit ahead of the second current sheet, but at nearly the same velocity. To some extent this behavior is commensurate with the concept of a $\mathbf{j} \times \mathbf{B}$ "piston" pushing a body of hot gas.

The other trajectory included in Figs. 6a and 6b (dashed line) is that predicted theoretically for a "snow-plow" type piston. In this theory, it is assumed that the current sheet is infinitesimally thin, completely impermeable to the gas it pushes, and that the accelerated gas accumulates in an

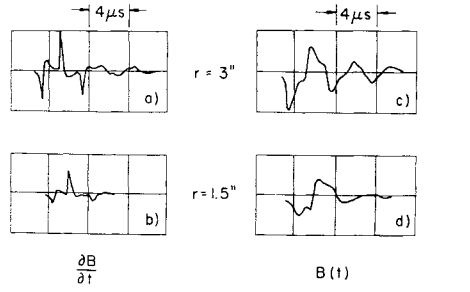

Fig. 5 Response of magnetic probes to pinch discharge in 20 μ argon.

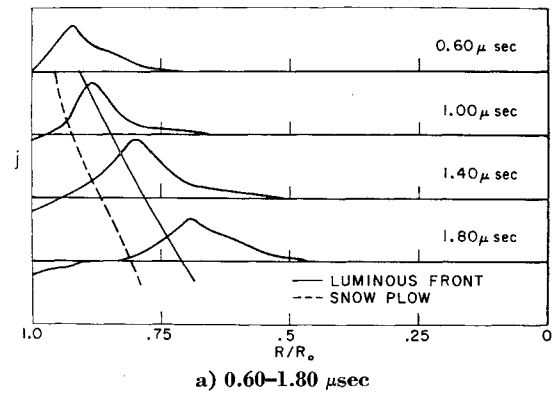

a) 0.60–1.80 μsec

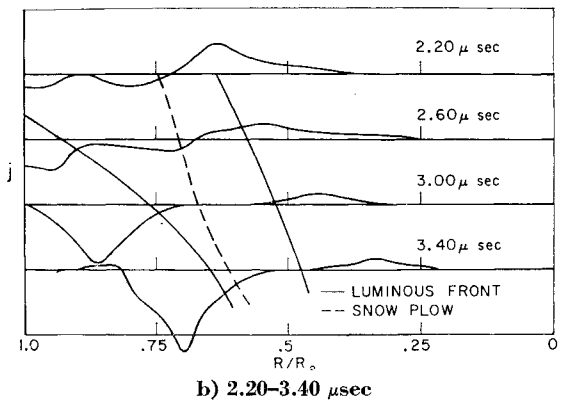

b) 2.20–3.40 μsec

Fig. 6 Radial current density distribution in 8-in. pinch discharge in 120 μ argon.

infinitesimally thin layer on the current sheet. This dynamical model is solved simultaneously with the circuit equation and with the statement of coaxial cylindrical inductance, for trajectories $r(t)$ of the current sheet, and for the ringdown pattern of the circuit. The details of this formulation are reviewed in the Appendix. Briefly, the problem is characterized by two dimensionless parameters and a dimensionless time:

$$\alpha = -\frac{\mu_0 h}{2\pi L_0} \qquad \beta = -\frac{Q_0^2}{4\pi\rho_0 r_0^4} \qquad \tau = \frac{t}{(L_0 C)^{1/2}}$$

where

h = distance between electrodes
L_0 = initial circuit inductance
Q_0 = initial charge on capacitors
ρ_0 = initial gas density
r_0 = radius of discharge at inception
C = capacitance of bank
t = real time

The parameter α essentially reflects the ratio of discharge inductance to external circuit inductance. For the prevailing experimental values, the trajectory solutions are relatively insensitive to α, other than through the implicit time scaling in L_0. The dynamical parameter β is much more manifest in the form of the solution. For large $|\beta|$ (>0.2), the current sheet reaches the center before the external current reverses. For small β, the external current reverses before the sheet reaches the center, a situation that we know experimentally causes a second breakdown at the periphery, thus clearly invalidating the theoretical model from that time.

Returning to Fig. 6, then, we compare the snow-plow trajectory for $\beta = -0.022$, the value prevailing in the experiment, with the observed current pulse. Over the first 2.2 μsec, where the theoretical model has some hope of applicability, the current pulse peak is seen to be substantially ahead of the snow-plow trajectory and to be traveling faster than it. The implications of this discrepancy will be discussed in the light of a broader range of scaling experiments described below.

Scaling Properties

Although a single set of experiments, such as that summarized in Fig. 6, leaves the applicability of the snow-plow concept considerably in doubt, the scaling relations that such a formulation yields seem sufficiently general to warrant experimental exploration. To this end, a variety of discharges have been produced, covering a range of the β parameter from -0.001 to -2.3. This variation can be achieved in several practical ways. Simplest is an adjustment of the initial gas density and molecular weight over the ranges where satisfactory discharges can be produced. To date, argon has been studied from 20 μ to 10 mm, nitrogen from 20 μ to 1 mm, and helium from 36 μ to 10 mm. Other ambient gas conditions are currently under study.

The β parameter varies as the square of the charge on the capacitor bank, and thus as the square of the capacitance, or the applied voltage. A certain amount of this type of survey has been performed, and more is in progress. It should be noted, however, that variation in bank capacitance also alters the time scaling factor, and variation in bank voltage may conceivably alter the nature of the breakdown initiation. For these reasons, this mode of scaling may be less instructive than the others.

The most significant factor in the β parameter is the initial discharge radius r_0, which appears in the inverse fourth power. By halving the radius of the discharge chamber, therefore, β is increased by a factor of 16, and substantial changes in the behavior of the discharge should appear. To explore this, one of the 8-in.-diam chambers was converted to a 4-in.

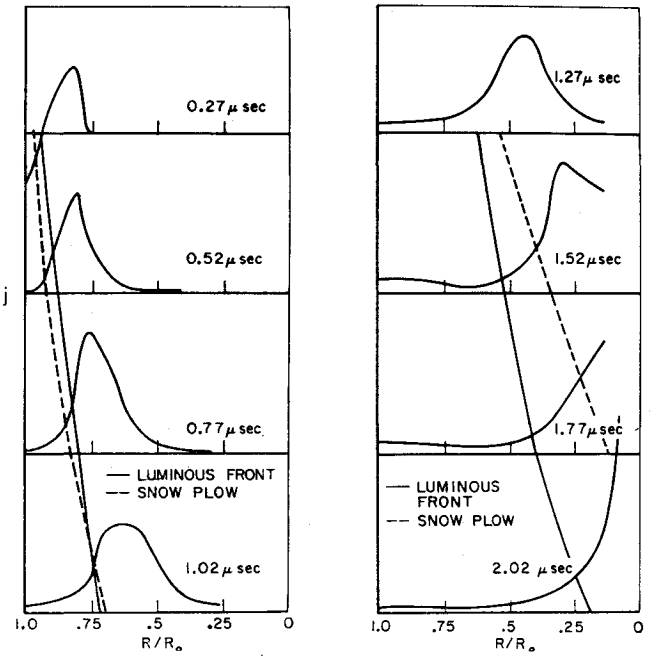

a) 0.27–1.02 μsec b) 1.27–2.02 μsec

Fig. 7 Radial current density distributions in 4-in. pinch discharge in 120 μ argon.

chamber by insertion of a suitable pyrex cylinder and plexiglas electrode shield. Discharges generated in this device were studied with the streak photography and magnetic probe techniques outlined previously. For argon, at all ambient pressures below 500 μ, the streak photographs reveal that the first luminous front is now much more intense and propagates more rapidly, accelerating over its entire radial course and reaching the center before current reversal in the external circuit. The secondary luminous fronts are relatively much less intense than in the larger chamber.

The magnetic probe records indicate a similar intensification of the first current pulse which is found to be narrower and steeper than the first pulse in the 8-in. machine and to

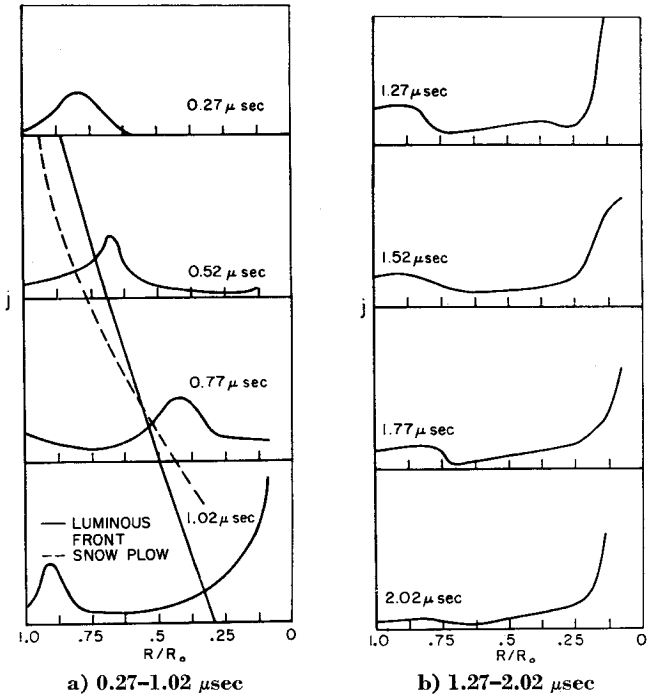

a) 0.27–1.02 μsec b) 1.27–2.02 μsec

Fig. 8 Radial current density distribution in 4-in. pinch discharge in 20 μ argon.

propagate all the way to the center. The secondary pulses produce much less pronounced responses on the magnetic probes. Figures 7a and 7b display the development of the current density profiles for a 120-μ discharge. The snow-plow calculations for the new appropriate value of $\beta = -0.36$ now yield a trajectory that is in much closer agreement with that of the observed current pulse. The luminous front follows the observed pulse and snow-plow trajectories for about 1.0 μsec and then falls somewhat behind.

Similar behavior is found at 20 μ, the lowest ambient pressure studied, where the current pulse now reaches the center in less than 1.0 μsec, i.e., before the external current has reached its first maximum (Figs. 8a and 8b). In this case, a second, positive pulse is found to originate at the outer wall at approximately the pinch time, but unlike the other secondary pulses, this one does not propagate away from the wall.

Figures 9a–10c present superpositions of the trajectories of the observed current pulse peaks and the theoretical snow-plow calculations for various pressures in the 8-in.- and 4-in.-diam discharges, respectively. In many cases, it is again

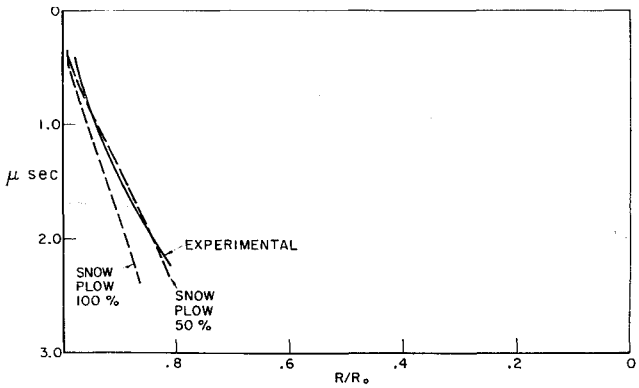

a) 480 μ

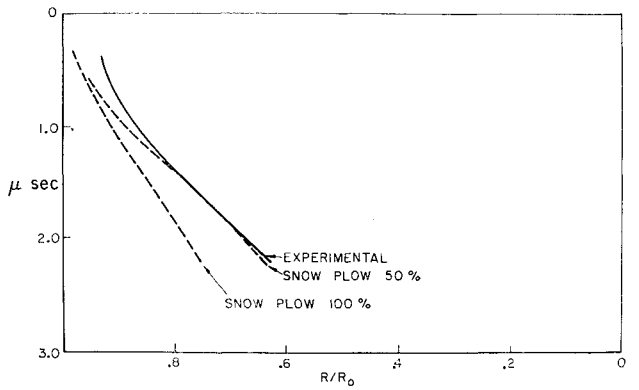

b) 120 μ

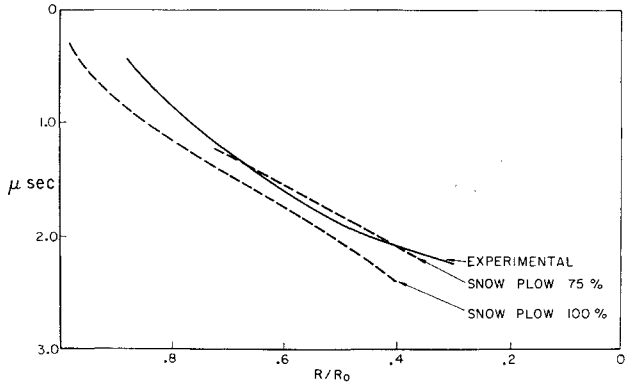

c) 30 μ

Fig. 9 Current pulse trajectories in 8-in. pinch discharge in argon.

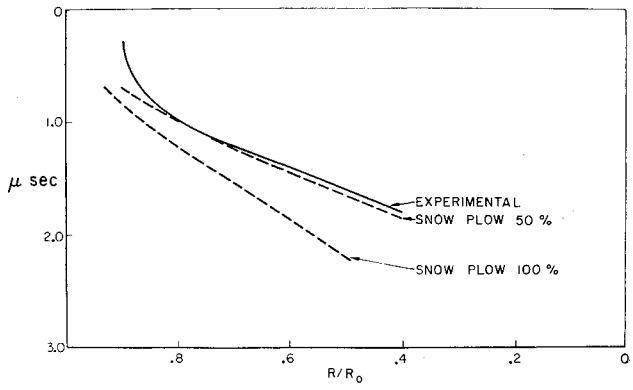

a) 500 μ

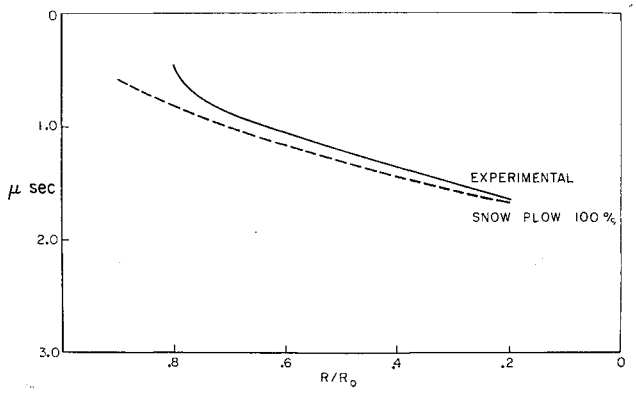

b) 120 μ

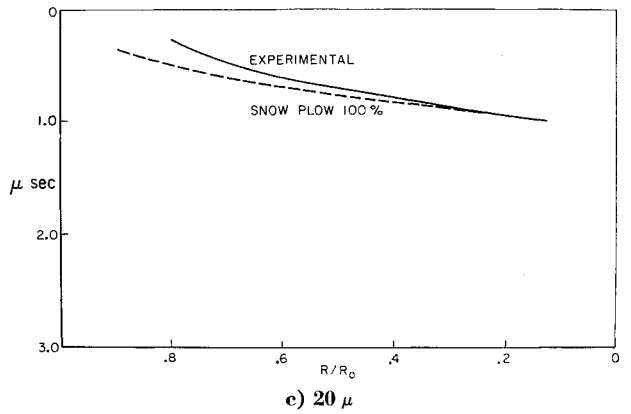

c) 20 μ

Fig. 10 Current pulse trajectories in 4-in. pinch discharge in argon.

found that the current pulses propagate somewhat faster than the theoretical trajectories, a property that could be construed as a failure of the current pulse to accelerate all of the gas it overruns, i.e., to a "leakiness" of the piston. A "leaky snow-plow" theory would differ from the more conventional one only in the appearance of a "sweeping efficiency" factor ξ in the denominator of the parameter, representing the fact that the piston only accumulates $\xi\rho_0$ of the original gas density as it propagates through it. Indeed, it is found that the snow-plow calculations can be brought into better coincidence with the experimental current pulse trajectories if higher values of β are empirically invoked. For example, in the 8-in. discharges in 480 and 120 μ argon (Figs. 9a and 9b), the experimental trajectories are found to correspond with the snow-plow trajectories for a value of β about twice that actually prevailing in the experiment, indicating about 50% sweeping efficiency ξ. For the same radius discharge at a lower pressure, 30μ (Fig. 9c), the correlation occurs for a theoretical β about $\frac{4}{3}$ that of the experiment, i.e., a 75% sweeping efficiency.

Similar comparisons for the 4-in.-diam discharges in argon, where the current density pulses are more intense, indicate higher sweeping efficiencies. At 20 and 120 μ, the correlation with the snow-plow model is within experimental error without any adjustment of β, i.e., the current pulse piston here seems to be essentially impermeable (Figs. 10b and 10c). At a higher pressure (500 μ), a 50% "inefficiency" again is indicated (Fig. 10a).

Summary

The experiments described here have revealed some aspects of the structure of the cylindrical current pulses arising in large-radius pinch discharges and the characteristics of their propagation toward the center. Comparison of these with the trajectories of the associated luminous fronts, and with the predictions of a simple snow-plow theory, suggests interpretation in terms of a porous piston action of the current pulses on the ambient gas. In the cases studied, the sweeping efficiency of the current pulses ranges from 50 to 100%, and seems to increase for lower ambient gas density and for smaller discharge radius.

Appendix: Snow-Plow Formulation of Pinch Dynamics[4]

Assume the discharge current to flow in one circular cylinder of infinitesimal thickness and infinite conductivity. Assume it collects all gas it passes over into one infinitesimally thin sheet coincident with itself. Let

r = radius of current sheet; initial value r_0
L_0 = inductance of external circuit
h = separation of electrodes
Q = charge on capacitors; initial value Q_0
ρ_0 = ambient gas density

The complete circuit relation

$$L\frac{d^2Q}{dt^2} + \frac{dL}{dt}\frac{dQ}{dt} + \frac{Q}{C} = 0 \tag{A1}$$

with the inductance in the form

$$L = L_0 + \frac{\mu_0 h}{2\pi}\ln\frac{r_0}{r} \tag{A2}$$

is to be solved simultaneously with the dynamical statement

$$\frac{d}{dt}\left[(r_0^2 - r^2)\frac{dr}{dt}\right] = -\frac{\mu_0(dQ/dt)^2}{4\pi^2\rho_0 r} \tag{A3}$$

Defining the five dimensionless parameters

$$\alpha = -\frac{\mu_0 h}{2\pi L_0} \qquad \beta = -\frac{Q_0^2}{4\pi^2\rho_0 r_0^4}$$

$$\tau = \frac{t}{(L_0 C)^{1/2}} \qquad y = \frac{r}{r_0} \qquad Z = \frac{Q}{Q_0}$$

yields the dimensionless circuit equation

$$\frac{d^2Z}{d\tau^2} + \frac{\alpha}{(1 + \alpha\ln y)y}\frac{dy}{d\tau}\frac{dZ}{d\tau} + \frac{Z}{(1 + \alpha\ln y)} = 0$$

with initial conditions

$$Z = 1 \qquad dZ/d\tau = 0 \quad \text{at} \quad \tau = 0$$

and the dimensionless momentum equation

$$\frac{d}{d\tau}\left[(1 - y^2)\frac{dy}{d\tau}\right] = \frac{\beta}{y}\left(\frac{dZ}{d\tau}\right)^2$$

with initial conditions

$$y = 1 \qquad dy/d\tau = 0 \quad \text{at} \quad \tau = 0$$

These relations were evaluated on an IBM 7090 for $y(\tau)$, $Z(\tau)$, $(dy/d\tau)(\tau)$, $(dZ/d\tau)(\tau)$, for a physically interesting range of α and β.

References

[1] Jahn, R. G. and von Jaskowsky, W., "Structure of a large-radius pinch discharge," AIAA J. **1**, 1809–1814 (1963).

[2] Jahn, R. G., von Jaskowsky, W., and Casini, A. L., "Gas-triggered inverse pinch switch," Rev. Sci. Instr. **34**, 1439–1440 (1963).

[3] Lovberg, R. H., "The use of magnetic probes in plasma diagnostics," Ann. Phys. **8**, 311–324 (1959).

[4] Rosenbluth, M., "Infinite conductivity theory of the pinch," Los Alamos TR LA-1850 (1954).